International Journal of Architectural, Civil and Construction Sciences
ISSN: 2415-1734
Vol:3, No:2, 2009

Mechanical Characteristics and Modeling of Multiple Trench Friction Pendulum System with Multi-intermediate Sliding Plates

C. S. Tsai, and Yung-Chang Lin

***Abstract*—**In order to upgrade the seismic resistibility of structures and enhance the functionality of an isolator, a new base isolator called the multiple trench friction pendulum system (MTFPS) is proposed in this study. The proposed MTFPS isolator is composed of a trench concave surface and several intermediate sliding plates in two orthogonal directions. Mathematical formulations have been derived to examine the characteristics of the proposed MTFPS isolator possessing multiple intermediate sliding plates. By means of mathematical formulations, it can be inferred that the natural period and damping effect of the MTFPS isolator with several intermediate sliding plates can be altered continually and controllably during earthquakes. Furthermore, results obtained from shaking table tests demonstrate that the proposed isolator provides good protection to structures for prevention of damage from strong earthquakes.

***Keywords*—**Friction Pendulum System; Multiple Friction Pendulum System; Base Isolation; Earthquake Engineering.

I. Introduction

THE base isolation technology has been recognized as a promising technique for the prevention of existing and new structures from earthquake damage. Among the base isolators developed in the past, a friction pendulum system (FPS) isolation device with a concave sliding surface and an articulated slider was proposed by Zayas in 1987 [1]. Through extensive experimental and numerical studies, the FPS isolator has been proven to be an efficient device for reduction of the seismic responses of structures [1–5]. Finite element formulations for a variable curvature friction pendulum system (VCFPS) have been presented by Tsai el al. in 2003 [6]. In order to enhance the earthquake proof efficiency and reduce the size of the FPS isolator, a multiple friction pendulum system (MFPS) with double concave surfaces and an articulated slider located between the concave surfaces was proposed by Tsai et al. in 2003 [7–12]. Seismic response characteristics of bridges using the multiple friction pendulum system with double concave surfaces have been reported by Kim and Yun in 2007 [13]. Furthermore, several other types of the MFPS isolator, which basically represent more than one pendulum system connected in series, were invented by Tsai in 2002 [14, 15]. Research conducted on the characteristics of the MFPS isolator has been published by Fenz and Constantinou in 2008 [16]. The efficiency of the MFPS isolator with four concave surfaces on seismic mitigation of buildings has been investigated by Morgan and Mahin in 2008 [17]. A direction-optimized friction pendulum system (DO-FPS) consisting of a spherical concave surface, a trench concave surface, and an articulated slider has been developed by Tsai et al. [15]. The DO-FPS isolator possesses important characteristics such as the natural period and damping effect, which are functions of the directional angle of the sliding motion of the articulated slider during earthquakes. Furthermore, a trench friction pendulum system (TFPS) that consists of one trench concave surface in the x and y directions and an articulated slider situated between the trench concave surfaces has been proposed by Tsai et al. [18, 19]. The TFPS possesses independent characteristics such as the natural period and damping effect in two orthogonal directions, which can be applied to a bridge or a structure with considerably different natural periods in two orthogonal directions.

In order to further enhance the functionality of the TFPS isolator, a new base isolation system called the multiple trench friction pendulum system (MTFPS) with multiple intermediate sliding plates is proposed in this study. As shown in Fig.1–5, the MTFPS isolator has multiple concave sliding interfaces that are composed of a trench concave surface, several intermediate sliding plates in each orthogonal direction, and an articulated slider located among the trench concave surfaces and intermediate sliding plates. The MTFPS represents more than one trench friction pendulum system connected in series in each orthogonal direction. The friction coefficient, displacement capacity, and radius of curvature of each trench concave surface or intermediate sliding plate in each direction can be different. The natural period and damping effect for a MTFPS isolator with several intermediate sliding plates change continually during earthquakes. Therefore, a large number of possibilities of combinations are available for engineering designs. Such options are dependent on the engineering

C.S. Tsai is with the Department of Civil Engineering, Feng Chia University, Taichung, Taiwan 40724 (corresponding author to provide phone: +886-4-24517250-3121;;fax:+886-4-24516982;e-mail:cstsai@fcu.edu.tw).

Y.C. Lin is with the Department of Civil Engineering, Feng Chia University, Taichung, Taiwan 40724 (corresponding author to provide phone: +886-4-24517250-4549;;fax:+886-4-24516982;e-mail:geonzaku@yahoo.com.tw).

requirements. In order

to examine the features of the new device, mathematical formulations have been derived in this study; to investigate the efficiency of the proposed MTFPS isolator in seismic mitigation for structures, a series of shaking table tests for a scaled steel structure equipped with the MTFPS isolators were carried out in the Department of Civil Engineering, Feng Chia University, Taichung, Taiwan. The results obtained from the experimental tests demonstrate that the MTFPS isolator with multiple intermediate sliding plates provides good protection for structures from earthquake damage.

II. Mathematical Formulations for MTFPS Isolator with Multiple Intermediate Sliding Plates

In order to study the characteristic of the MTFPS isolator with multiple intermediate sliding plates, mathematical formulations have been derived as follows. Fig. 6 shows a MTFPS isolator having one trench concave surface and two intermediate sliding plates to form three sliding interfaces in the X direction. The radii of curvature of the first, second, and third sliding interfaces are R_{x1}, R_{x2}, and R_{x3}, respectively. The friction coefficients of the first, second, and third sliding interfaces are μ_{x1}, μ_{x2}, and μ_{x3}, respectively. The displacement capacities on the 1st, 2nd, and 3rd sliding interfaces are d_{x1}, d_{x2}, and d_{x3}, respectively. In the following derivations, we assume the following conditions: (a) $R_{x1} > R_{x2} > R_{x3}$; (b) $\mu_{x1} > \mu_{x2} > \mu_{x3}$; and (c) $d_{xi} > (\mu_{x(i-1)} - \mu_{xi})R_{xi}$. Fig. 7 (a) and (b) show the forces acting on the 3rd sliding interface in the X direction when the sliding motion is initiated on the 3rd sliding interface with the least friction coefficient. F_x denotes the mobilized force in the X direction; u_x, the total displacement of the articulated slider in the X direction; u_{xi}, the displacement on the i*th* sliding interface in the X-direction; S_{xi}, the force normal to the i-*th* sliding interface in the X-direction; F_{fxi}, the frictional force in the direction tangential to the i-*th* sliding interface; W, the vertical force resulting from the superstructure including the static and dynamic loadings; and θ_{xi}, the rotation angle in the X-direction on the i-*th* sliding interface relative to the vertical direction. The sliding sequence of the components of the MTFPS isolator is determined by the friction coefficients and the radii of the sliding interfaces. The sliding motion is initiated on the i-*th* sliding interface when the horizontally mobilized force, F_x, exceeds the frictional force on the i-*th* sliding interface, F_{fxi}.

In stage Ⅰ, when $F_{fx3} \leqq F_x < F_{fx2}$, the articulated slider starts sliding on the 3rd sliding interface. As shown in Fig. 7 (a) and (b), from the equilibrium equation in the X-direction and by neglecting the frictional forces from the walls of intermediate plates, the governing equation in the horizontal direction is expressed as

$$F_x - S_{x3}\sin\theta_{x3} - F_{fx3}\cos\theta_{x3} = 0 \quad (1)$$

The governing equation in the vertical direction is obtained as

$$W - S_{x3}\cos\theta_{x3} + F_{fx3}\sin\theta_{x3} = 0 \quad (2)$$

Rearrangement of Equation (2) results in the following expression:

$$S_{x3} = \frac{W + F_{fx3}\sin\theta_{x3}}{\cos\theta_{x3}} \quad (3)$$

Back-substitution of Equation (3) into Equation (1) leads to

$$F_x = W\tan\theta_{x3} + \frac{F_{fx3}}{\cos\theta_{x3}} = W\frac{\sin\theta_{x3}}{\cos\theta_{x3}} + \frac{F_{fx3}}{\cos\theta_{x3}} \quad (4)$$

If the displacement is small, i.e., if $\theta_{x3} \approx 0$ and $\cos\theta_{x3} \approx 1$, Equation (4) can be rewritten as follows:

$$F_x = W\sin\theta_3 + F_{fx3} = \frac{W}{R_{x3}}u_{x3} + F_{fx3} \quad (5)$$

where

$$\sin\theta_{x3} = \frac{u_{x3}}{R_{x3}} \quad (6)$$

The total displacement in the X direction is obtained as $u_x = u_{x1} + u_{x2} + u_{x3} = 0 + 0 + u_{x3}$.

Equation (5) can be rewritten as

$$F_x = \frac{W}{R_{x3}}u_x + F_{fx3} \quad (7)$$

and the hysteretic behavior of the MTFPS isolator is illustrated in Fig. 8.

In stage Ⅱ, as shown in Fig. 9, when $F_x = F_{fx2}$, the sliding motion on the 3rd sliding interface will stop, and the 2nd sliding interface will start sliding.

The mobilized force under such conditions is expressed as follows:

$$F_x = \frac{W}{R_{x3}}u_x + F_{fx3} = F_{fx2} \quad (8)$$

and the transition action occurs at displacement u_x^*, expressed by

$$u_x^* = (F_{fx2} - F_{fx3})\frac{R_{x3}}{W} = (\mu_{x2} - \mu_{x3})R_{x3} \quad (9)$$

When $F_{fx2} \leqq F_x < F_{fx1}$, the mobilized force on the 2nd sliding interface is given by

$$F_x = \frac{W}{R_{x2}}u_{x2} + F_{fx2} \quad (10)$$

On the 3rd sliding interface, the governing equation in the horizontal direction is expressed as

$$F_x - S_{x3}\sin(\theta_{x2} + \theta_{x3}) - F_{fx3}\cos(\theta_{x2} + \theta_{x3}) = 0 \quad (11)$$

and the governing equation in the vertical direction is obtained as

$$F_x = \frac{W}{R_{x2}}u_{x2} + F_{fx2} \quad (12)$$

The solution to Equations (12) and (13) is given by

$$F_x = W\tan(\theta_{x2}+\theta_{x3}) + \frac{F_{fx3}}{\cos(\theta_{x2}+\theta_{x3})} = W\frac{\sin(\theta_{x2}+\theta_{x3})}{\cos(\theta_{x2}+\theta_{x3})} + \frac{F_{fx3}}{\cos(\theta_{x2}+\theta_{x3})} \quad (13)$$

If the displacement is small, i.e., if $\theta_{x2} \approx \theta_{x3} \approx 0$, then, $\cos\theta_{x2} \approx \cos\theta_{x3} \approx 1$ and $\sin\theta_{x2}\sin\theta_{x3} \approx 0$.

Equation (13) can be rewritten as

$$F_x = W(\sin\theta_{x2} + \sin\theta_{x3}) + F_{fx3} = W\left(\frac{u_{x2}}{R_{x2}} + \frac{u_{x3}}{R_{x3}}\right) + F_{fx3} \quad (14)$$

Substitution of Equation (10) into Equation (14) yields

$$u_{x3} = (F_{fx2} - F_{fx3})\frac{R_{x3}}{W} = (\mu_{x2} - \mu_{x3})R_{x3} = constant \quad (15)$$

The result in Equation (15) implies that the displacement on the 3rd sliding interface is constant and that the sliding motion on the 3rd sliding interface stops in this stage.

Substitution of Equation (15) into Equation (14) yields

$$u_{x2} = (F_x - \mu_{x2}W)\frac{R_{x2}}{W} = (F_x - F_{fx2})\frac{R_{x2}}{W} \quad (16)$$

The total displacement obtained as $u_x = u_{x1} + u_{x2} + u_{x3}$, and $u_x = 0 + u_{x2} + u_{x3}$ in the X direction, and rearrangement of Equations (15) and (16) yields

$$\begin{aligned} F_x &= \frac{W}{R_{x2}}[u_x - u_{x1} - u_{x3}] + F_{fx2} \\ &= \frac{W}{R_{x2}}[u_x - (\mu_{x2} - \mu_{x3})R_{x3}] + F_{fx2} \\ &= \frac{W}{R_{x2}}u_x + \left[\frac{F_{fx2}(R_{x2} - R_{x3}) + F_{fx3}R_{x3}}{R_{x2}}\right] \end{aligned} \quad (17)$$

The hysteretic behavior of the MTFPS isolator in this stage is demonstrated in Fig. 10.

In stage III, as shown in Fig. 11, when $F_x = F_{fx1}$, the sliding motion on the 2nd sliding interface stops and the 1st sliding interface starts sliding.

By using Equation (17), the mobilized force under the abovementioned conditions is obtained as

$$F_{fx1} = \frac{W}{R_{x2}}u_x + \frac{F_{fx2}(R_{x2} - R_{x3}) + F_{fx3}R_{x3}}{R_{x2}} \quad (18)$$

and this transition action occurs at displacement u_x^{**}, expressed as

$$\begin{aligned} u_x^{**} &= \left[F_{fx1} - \frac{F_{fx2}(R_{x2} - R_{x3}) + F_{fx3}R_{x3}}{R_{x2}}\right]\frac{R_{x2}}{W} \\ &= (\mu_{x1} - \mu_{x2})R_{x2} + (\mu_{x2} - \mu_{x3})R_{x3} \end{aligned} \quad (19)$$

When $F_{fx1} \leqq F_x$, the mobilized force on the 1st interface is obtained as

$$F_x = \frac{W}{R_{x1}}u_{x1} + F_{fx1} \quad (20)$$

As shown in Fig. 11c, on the 2nd sliding interface, the governing equation in the horizontal direction is expressed as follows:

$$F_x - S_{x2}\sin(\theta_{x1}+\theta_{x2}) - F_{fx2}\cos(\theta_{x1}+\theta_{x2}) = 0 \quad (21)$$

and the governing equation in the vertical direction is obtained as

$$W - S_{x2}\cos(\theta_{x1}+\theta_{x2}) + F_{fx2}\sin(\theta_{x1}+\theta_{x2}) = 0 \quad (22)$$

The solution to Equations (21) and (22) is expressed as

$$F_x = W\sin(\theta_{x1}+\theta_{x2}) + F_{fx2} = W\left(\frac{u_{x1}}{R_{x1}} + \frac{u_{x2}}{R_{x2}}\right) + F_{fx2} \quad (23)$$

As shown in Fig. 11d, on the 3rd sliding interface, the governing equation in the horizontal direction is given by

$$F_x - S_{x3}\sin(\theta_{x1}+\theta_{x2}+\theta_{x3}) - F_{fx3}\cos(\theta_{x1}+\theta_{x2}+\theta_{x3}) = 0 \quad (24)$$

and the governing equation in the vertical direction is obtained as

$$F_x - S_{x3}\sin(\theta_{x1}+\theta_{x2}+\theta_{x3}) - F_{fx3}\cos(\theta_{x1}+\theta_{x2}+\theta_{x3}) = 0 \quad (25)$$

Combining Equations (25) and (26) yields

$$\begin{aligned} F_x &= W\tan(\theta_{x1}+\theta_{x2}+\theta_{x3}) + \frac{F_{fx3}}{\cos(\theta_{x1}+\theta_{x2}+\theta_{x3})} \\ &= W\frac{\sin(\theta_{x1}+\theta_{x2}+\theta_{x3})}{\cos(\theta_{x1}+\theta_{x2}+\theta_{x3})} + \frac{F_{fx3}}{\cos(\theta_{x1}+\theta_{x2}+\theta_{x3})} \end{aligned} \quad (26)$$

For small displacements, we have Equations (27) and (28).

$$\begin{aligned} &\sin(\theta_{x1}+\theta_{x2}+\theta_{x3}) \\ &= \sin\theta_{x1}\cos\theta_{x2}\cos\theta_{x3} - \sin\theta_{x1}\sin\theta_{x2}\sin\theta_{x3} \\ &+ \cos\theta_{x1}\sin\theta_{x2}\cos\theta_{x3} + \cos\theta_{x1}\cos\theta_{x2}\sin\theta_{x3} \\ &\approx \sin\theta_{x1} + \sin\theta_{x2} + \sin\theta_{x3} \end{aligned} \quad (27)$$

and

$$\begin{aligned} &\cos(\theta_{x1}+\theta_{x2}+\theta_{x3}) = \cos\theta_{x1}\cos\theta_{x2}\cos\theta_{x3} - \sin\theta_{x1}\sin\theta_{x2}\cos\theta_{x3} \\ &- \sin\theta_{x1}\cos\theta_{x2}\sin\theta_{x3} - \cos\theta_{x1}\sin\theta_{x2}\sin\theta_{x3} \\ &\approx 1 \end{aligned} \quad (28)$$

By virtue of Equations (27) and (28), Equation (26) can be rewritten as

$$\begin{aligned} &\cos(\theta_{x1}+\theta_{x2}+\theta_{x3}) = \cos\theta_{x1}\cos\theta_{x2}\cos\theta_{x3} - \sin\theta_{x1}\sin\theta_{x2}\cos\theta_{x3} \\ &- \sin\theta_{x1}\cos\theta_{x2}\sin\theta_{x3} - \cos\theta_{x1}\sin\theta_{x2}\sin\theta_{x3} \\ &\approx 1 \end{aligned} \quad (29)$$

Substitution of Equation (23) into Equation (29) yields

$$u_{x3} = (F_{fx2} - F_{fx3})\frac{R_{x3}}{W} = (\mu_{x2} - \mu_{x3})R_{x3} \quad (30)$$

Substitution of Equation (20) into Equation (23) leads to

$$u_{x2} = (F_{fx1} - F_{fx2})\frac{R_{x2}}{W} = (\mu_{x1} - \mu_{x2})R_{x2} \quad (31)$$

The total displacement in the X direction is obtained as $u_x = u_{x1} + u_{x2} + u_{x3}$.

Combination of Equations (20), (30), and (31) results in

$$\begin{aligned} F_x &= \frac{W}{R_{x1}}[u_x - u_{x2} - u_{x3}] + F_{fx1} \\ &= \frac{W}{R_{x1}}u_x + \frac{F_{fx1}(R_{x1} - R_{x2}) + F_{fx2}(R_{x2} - R_{x3}) + F_{fx3}R_{x3}}{R_{x1}} \end{aligned} \quad (32)$$

The hysteretic behavior of the MTFPS isolator in this stage is shown in Fig. 12.

In stage IV, as shown in Fig. 13, when contact is made with the displacement restrainer on the 1st sliding interface, the sliding motion on the 1st sliding interface stops and the sliding of the 2nd sliding interface is restarted. The displacement on the 1st sliding interface, u_{x1}, is equal to d_{x1} and the mobilized

force, F_{xrd1}, under such conditions is given by

$$F_{xrd1} = \frac{W}{R_{x1}} d_{x1} + F_{fx1} \tag{33}$$

This transition action occurs at the total displacement, u_{xdr1}, expressed as

$$F_{xrd1} = \frac{W}{R_{x1}} d_{x1} + F_{fx1} \tag{34}$$

After the contact, the mobilized force on the 2nd sliding interface is obtained as

$$F_{xrd1} = \frac{W}{R_{x1}} d_{x1} + F_{fx1} \tag{35}$$

The mobilized force on the 3rd sliding interface is given by

$$F_x = W(\frac{d_{x1}}{R_{x1}} + \frac{u_{x2}}{R_{x2}} + \frac{u_{x3}}{R_{x3}}) + F_{f3} \tag{36}$$

Back-substitution of Equation (36) into Equation (35) leads to

$$u_{x3} = \frac{R_{x3}}{W}(F_{fx2} - F_{fx3}) = (\mu_{x2} - \mu_{x3})R_{x3} \tag{37}$$

The total displacement $u_x = u_{x1} + u_{x2} + u_{x3}$; therefore, $u_{x2} = u_x - d_{x1} - u_{x3}$, and back-substitution of Equation (37) into Equation (35) leads to

$$\begin{aligned} F_x &= \frac{W}{R_{x2}}[u_x - u_{x1} - u_{x3}] + W\frac{d_{x1}}{R_{x1}} + F_{fx2} \\ &= \frac{W}{R_{x2}}[u_x - d_{x1} - (\mu_{x2} - \mu_{x3})R_{x3}] + W\frac{d_{x1}}{R_{x1}} + F_{fx2} \end{aligned} \tag{38}$$

The hysteretic behavior of the MTFPS isolator in this stage is shown in Fig. 14.

In stage Ⅴ, as shown in Fig. 15, when contact is made with the displacement restrainer on sliding interface 2, the sliding motion on the 2nd sliding interface stops and the sliding of the 3rd sliding interface is restarted. The displacement on the 1st sliding interface, u_{x1}, is equal to d_{x1}, and the displacement on the 2nd sliding interface, u_{x2}, is equal to d_{x2}. The mobilized force is expressed as

$$F_{xdr2} = W(\frac{d_{x1}}{R_{x1}} + \frac{d_{x2}}{R_{x2}}) + F_{fx2} \tag{39}$$

By back-substituting Equation (39) into Equation (38), we obtain the transition displacement in total, u_{xdr2}, as follows:

$$\begin{aligned} u_{xdr\,2} &= d_{x1} + (\mu_{x2} - \mu_{x3})R_{x3} + (\frac{d_{x1}}{R_{x1}} + \frac{d_{x2}}{R_{x2}})R_{x2} \\ &= d_{x1} + d_{x2} + (\mu_{x2} - \mu_{x3})R_{x3} \end{aligned} \tag{40}$$

We obtain the total displacement $u_x = u_{x1} + u_{x2} + u_{x3}$; therefore, $u_{x3} = u_x - d_{x1} - d_{x2}$, and rewriting Equation (36) leads to

$$\begin{aligned} F_x &= W\frac{u_{x3}}{R_{x3}} + W(\frac{d_{x1}}{R_{x1}} + \frac{d_{x2}}{R_{x2}}) + F_{fx3} \\ &= \frac{W}{R_{x3}}(u_x - d_{x1} - d_{x2}) + W(\frac{d_{x1}}{R_{x1}} + \frac{d_{x2}}{R_{x2}}) + F_{fx3} \end{aligned} \tag{41}$$

The hysteretic behavior of the MTFPS isolator in this stage is shown in Fig. 16.

By observing the mobilized force and the displacement at each sliding interface from stageⅠ to stageⅤ, we can find the regularities and further infer the regular pattern of an MTFPS isolator with several intermediate sliding plates. If the isolation system has N number of sliding interfaces and by assuming the following conditions: (a) $R_{x1} > R_{x2} > R_{x3} > ... > R_{xj} > ... > R_{xN}$, (b) $\mu_{x1} > \mu_{x2} > \mu_{x3} > .... > \mu_{xj} > ... > \mu_{xN}$,(c) $d_{xi} > (\mu_{x(i-1)} - \mu_{xi})R_{xi}$, the following equations can be obtained.

When the sliding motion occurs on the j-*th* sliding interface without contacting the displacement restrainer, the 1st to the (j - 1)-*th* sliding interfaces remain standing still without any movement. The (j + 1)-*th* sliding interface to the N-th sliding interfaces have already stopped, and the displacement in each sliding interface is expressed as follows:

When $1 \le i < j$, $u_{xi} = 0$; and (42)

when $j < i \le N$, $u_{xi} = (\mu_{x(i-1)} - \mu_{xi})R_{xi}$ (43)

The mobilized force is given by

$$\begin{aligned} F_x &= \frac{W}{R_{xj}}[u_x - u_{x1} - u_{x2} - ... - u_{x(j-1)} - u_{x(j+1)} - .... - u_{xN}] + F_{fxj} \\ &= \frac{W}{R_{xj}}[u_x - (\mu_{xj} - \mu_{x(j+1)})R_{x(j+1)} - (\mu_{x(j+1)} - \mu_{x(j+2)})R_{x(j+2)} \\ &\quad - .....- (\mu_{x(N-1)} - \mu_{x(N)})R_{xN}] + F_{fxj} \\ &= \frac{W}{R_{xj}}u_x + \frac{F_{fxj}(R_{xj} - R_{x(j+1)}) + F_{fx(j+1)}(R_{x(j+1)} - R_{x(j+2)}) + ... + F_{fxN}R_{xN}}{R_{xj}} \end{aligned} \tag{44}$$

When contact is made with the displacement restrainer on the sliding interface j - 1, the displacement capacities are reached from the 1st to the (j - 1)-*th* sliding interfaces. The sliding motion occurs on the j*th* sliding interface, and the displacement in each sliding interface is expressed as

When $1 \le i < j$, $u_{xi} = d_{xi}$; and (45)

when $(j+1) \le i \le N$, $u_{xi} = (\mu_{x(i-1)} - \mu_{xi})R_{xi}$ (46)

and the mobilized force can be expressed as follows:

$$\begin{aligned} F_x &= \frac{W}{R_{xj}}[u_x - u_{x1} - u_{x2} - ... - u_{x(j-1)} - u_{x(j+1)} - .... - u_{xN}] + F_{fxj} \\ &= \frac{W}{R_{xj}}[u_x - (\mu_{xj} - \mu_{x(j+1)})R_{x(j+1)} - (\mu_{x(j+1)} - \mu_{x(j+2)})R_{x(j+2)} \\ &\quad - .....- (\mu_{x(N-1)} - \mu_{x(N)})R_{xN}] + F_{fxj} \\ &= \frac{W}{R_{xj}}u_x + \frac{F_{fxj}(R_{xj} - R_{x(j+1)}) + F_{fx(j+1)}(R_{x(j+1)} - R_{x(j+2)}) + ... + F_{fxN}R_{xN}}{R_{xj}} \end{aligned} \tag{47}$$

Similarly, by following the same procedures as those corresponding to Equations (1)–(47) in the X direction, mathematical formulations in the Y direction can be obtained. This means that by neglecting frictional forces from the walls of the intermediate sliding plates, the proposed MTFPS isolator with multiple intermediate sliding plates will move independently in two orthogonal directions. Accordingly, the natural period and damping effect of the isolator in each direction will change at various stages during earthquakes.

III. Shaking Table Tests on a Three- story Steel Structure Isolated with MTFPS Isolators

In order to examine the efficiency of the proposed isolator on seismic mitigation, a series of shaking table tests on a three-story scaled steel structure isolated with MTFPS were performed in the Department of Civil Engineering, Feng Chia University, Taichung, Taiwan. The sizes of the three-story steel structure were 1.1 m × 1.1 m on the horizontal plane and 2.7 m in height. The cross-section of the column on each floor was H100 × 50 × 5 × 7 mm. In order to simulate inertial forces on each floor, an additional mass of 400 kg was added on each floor. The total mass, including the mass of the structure and added masses, was approximately 2.0 tons, as shown in Fig. 17. In the experiment, selected ground motions including the El Centro (US, 1940), Kobe (Japan, 1995), and Chi-Chi earthquakes (the TCU084 station, Taiwan, 1999) were selected as inputs. The PGA of the input ground motions varied from 0.2 g to 0.6 g. An MTFPS isolator was installed at the bottom of each column. The MTFPS isolator used in this test had one trench concave surface and one intermediate sliding plate to form two sliding interfaces in each direction. The radii of curvature of the 1st and 2nd sliding interfaces were 1 m and 0.5 m, respectively. The friction coefficients at low velocities for the 1st and 2nd sliding interfaces were 0.037 and 0.0356, respectively, and 0.107 and 0.103 at high velocities for the 1st and 2nd sliding interfaces, respectively. The accelerometers and the displacement transducers (LVDT) were deployed at each floor and the shaking table to measure the structural responses and ground motions.

Fig. 18–20 display comparisons between the roof acceleration responses of the fixed-base and MTFPS-isolated structures under the El Centro, Kobe and Chi-Chi (TCU084 station) earthquakes with 0.6 g in PGA, respectively. From these figures, it can be observed that the MTFPS isolator can significantly reduce structural responses by lengthening the natural period of the entire system and by supplying additional damping under various types of ground motions. The hysteresis loops of the MTFPS isolator under various earthquakes are shown in Fig. 21–23. The enclosed area of the hysteresis loop provides the damping effect to minimize the structural response and the isolator displacement. The test results indicate that the proposed isolator can isolate and absorb earthquake-induced energy. Fig. 24–26 shows the displacement time history of the MTFPS isolator when subjected to various earthquakes. It is demonstrated from these figures that negligible residual displacements are observed after earthquakes. Table I summarizes the comparisons between the roof acceleration responses of the fixed-base and MTFPS-isolated structures. The higher the intensity of the ground motion, the better will be the efficiency of the MTFPS isolator to reduce structural responses. It is also illustrated that the proposed MTFPS isolator is a promising tool for seismic mitigation of structures.

IV. Conclusion

The characteristics of the proposed multiple trench friction pendulum system with multiple intermediate sliding plates are generally functions of radii and friction coefficients of the trench concave surface and intermediate sliding plates in each direction. The new system provides large flexibility of serving different designing requirements for engineers. The MTFPS isolator moving independently in two orthogonal directions can provide different natural periods, displacement capacities, and damping effects in each direction. The natural period and damping effect of the MTFPS isolator with multiple intermediate sliding plates can change continually during earthquakes. This might avoid the possibility of resonance induced by the ground motions. The shaking table test results demonstrate that the proposed MTFPS isolator can reduce structural responses significantly and that the MTFPS isolator is a promising tool for protection of structures from earthquake damage.

References

[1] Zayas VA, Low SS and Mahin SA. The FPS earthquake resisting system report. *EERC Technical Report*, UBC/EERC-87/01, 1987.
[2] Tsai CS. Seismic behavior of buildings with FPS isolators. Second Congress on Computing in Civil Engineering (ASCE), Atlanta, GA, 1995; 1203-1211.
[3] Tsai CS. Finite element formulations for friction pendulum isolation bearings. International Journal for Numerical Method in Engineering 1997; 40:29-49.
[4] Al-Hussaini TM, Zayas VA and Constantinou MC. Seismic isolation of multi-story frame structures using spherical sliding isolation systems. Technical Report, NCEER-94-0007, 1994.
[5] Jangid RS. Optimum friction pendulum system for near-fault motions. Engineering Structures 2005; 27:349-359.
[6] Tsai CS, Chiang TC and Chen BJ. Finite element formulations and theoretical study for variable curvature friction pendulum system. Engineering Structures 2003; 25:1719-1730.
[7] Tsai CS, Chiang TC and Chen BJ. Seismic behavior of MFPS isolated structure under near-fault sources and strong ground motions with long predominant periods. In: the 2003 ASME Pressure Vessels and Piping Conference, Seismic Engineering, Chen, J. C. (ed.), Cleveland, Ohio, U. S. A., July, 2003; 466:73-79.
[8] Tsai CS, Chiang TC and Chen BJ. Shaking table tests of a full scale steel structure isolated with MFPS. In: the 2003 ASME Pressure Vessels and Piping Conference, Seismic Engineering, Chen, J. C. (ed.), Cleveland, Ohio, U. S. A., July, 2003; 466:41-47.
[9] Tsai CS, Chen BJ, Pong WS and Chiang TC. Interactive behavior of structures with multiple friction pendulum isolation system and unbounded foundations", Advances in Structural Engineering, An International Journal 2004; 7(6):539-551.
[10] Tsai CS, Chiang TC, Chen BJ. Experimental evaluation piecewise exact solution for predicting seismic responses of spherical sliding type isolated structures. Earthquake Engineering and Structural Dynamics 2005; 34(9):1027–1046.
[11] Tsai CS, Cheng CK, Chen MJ and S. H. Yu SH. Experimental study of MFPS-isolated sensitive equipment. In: the 2003 ASME Pressure Vessels and Piping Conference, Seismic Engineering, ASME, Edited by C. S. Tsai, Denver, Colorado, U.S.A., July 17-21, 2005, 8:11-18.
[12] Tsai CS, Chen WS, Chiang TC and Chen BJ. Component and shaking table tests for full-scale multiple friction pendulum system. Earthquake Engineering and Structural Dynamics 2006; 35(11):1653–1675.
[13] Kim YS and Yun CB. Seismic response characteristics of bridges using double concave friction pendulum bearings with tri-linear behavior. Engineering Structures 2007; 29:3082-3093.
[14] Tsai, CS. Improved structures of base isolation systems. Taiwan Patent No. 207126, Publication Number 00542278, Publication Date: July 11, 2003, Application Number 091210175, Filing date: July4, 2002 [in Chinese].

[15] Tsai CS, Lu PC, Chen W S, Chiang TC, Yang CT and Lin YC. Finite element formulation and shaking table tests of direction-optimized friction pendulum system. Engineering Structures 2008; 30:2321-2329.
[16] Fenz DM and Constantinou MC. Spherical sliding isolation bearings with adaptive behavior: Theory. Earthquake Engineering and Structural Dynamics 2008; 37:168-183.
[17] Morgan TA and Mahin SA. The optimization of multi-stage friction pendulum isolators for loss mitigation considering a range of seismic hazard. In: the 14th World Conference on Earthquake Engineering, Beijing, China, October 12-17, 2008; Paper No. 11-0070.
[18] Tsai, CS, Lu PC and Chen WS. Shaking table tests of a building isolated with a trench friction pendulum system. In: the 2006 ASME Pressure Vessels and Piping Conference, Seismic Engineering, Cory, James. F. (ed.), Vancouver, BC, Canada, July, 2006; Paper No. PVP2006-ICPVT11-93253.
[19] Tsai CS, Lin YC and Chen WS. Seismic behavior of high-tech facility isolated with a trench friction pendulum system. In: the 2006 ASME Pressure Vessels and Piping Conference, Seismic Engineering, Cory, James. F. (ed.), Vancouver, BC, Canada, July, 2006; Paper No. PVP2006-ICPVT11-93474.

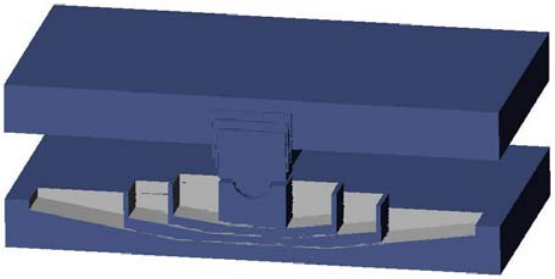

Fig. 1 Cross sectional view of multiple trench friction pendulum system

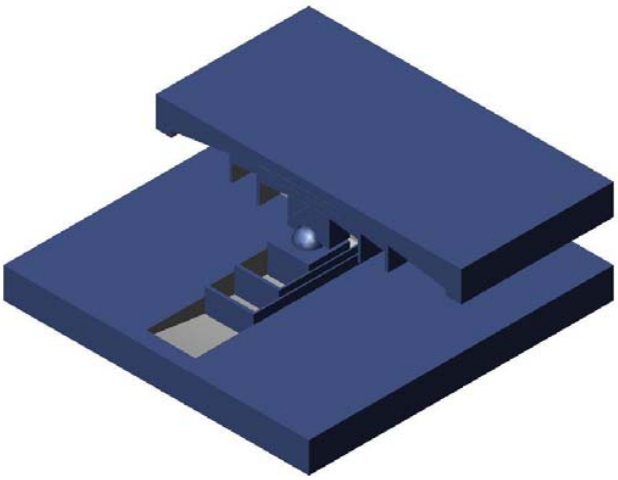

Fig. 2 Exploded view of MTFPS Isolator

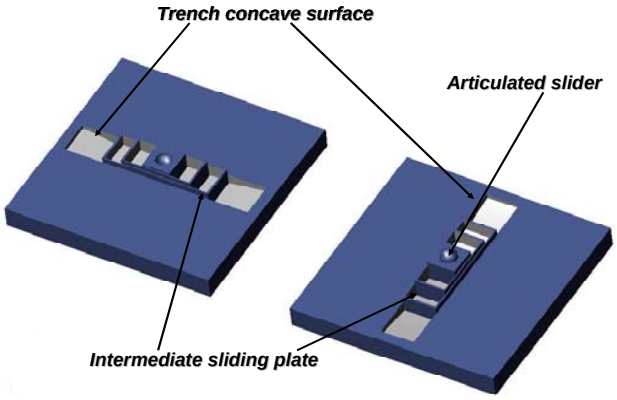

Fig. 3 Open-up view of MTFPS Isolator

TABLE I
COMPARISON OF ROOF ACCELERATION RESPONSES OF THE FIXED-BASE AND MTFPS-ISOLATED STRUCTURES

EARTHQUAKE	PGA (G)	FIXED-BASE STRUCTURE (G)	MTFPS-ISOLATED STRUCTURE (G)	RESPONSE REDUCTION
EL CENTRO	0.182	0.613	0.168	72.60 %
	0.301	1.012	0.232	77.12 %
	0.564	1.900	0.236	87.58 %
	0.619	2.085	0.285	86.31 %
KOBE	0.186	0.391	0.182	53.52 %
	0.279	0.585	0.203	65.29 %
	0.357	0.749	0.211	71.76 %
	0.602	1.264	0.259	79.50 %
CHI-CHI (TCU084)	0.196	0.391	0.170	56.67 %
	0.338	0.673	0.192	71.53 %
	0.399	0.796	0.234	70.55 %
	0.540	1.076	0.242	77.49 %

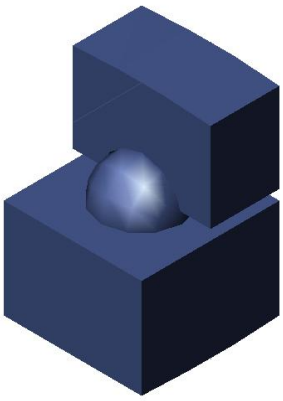

Fig. 4 Exploded view of articulated slider

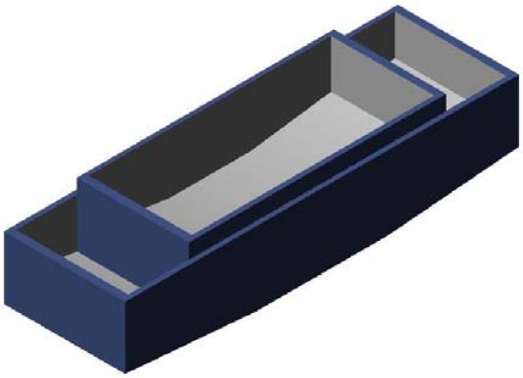

Fig. 5 Intermediate sliding plates

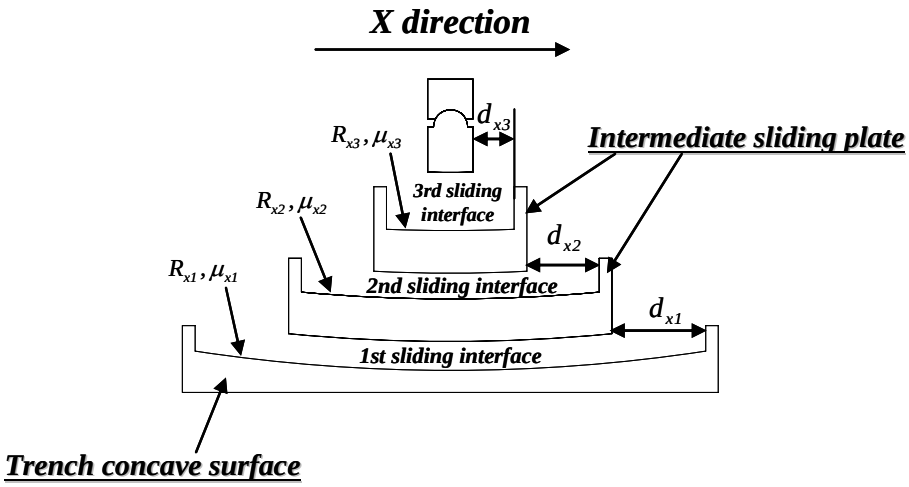

Fig. 6 Properties of sliding interfaces in MTFPS isolator

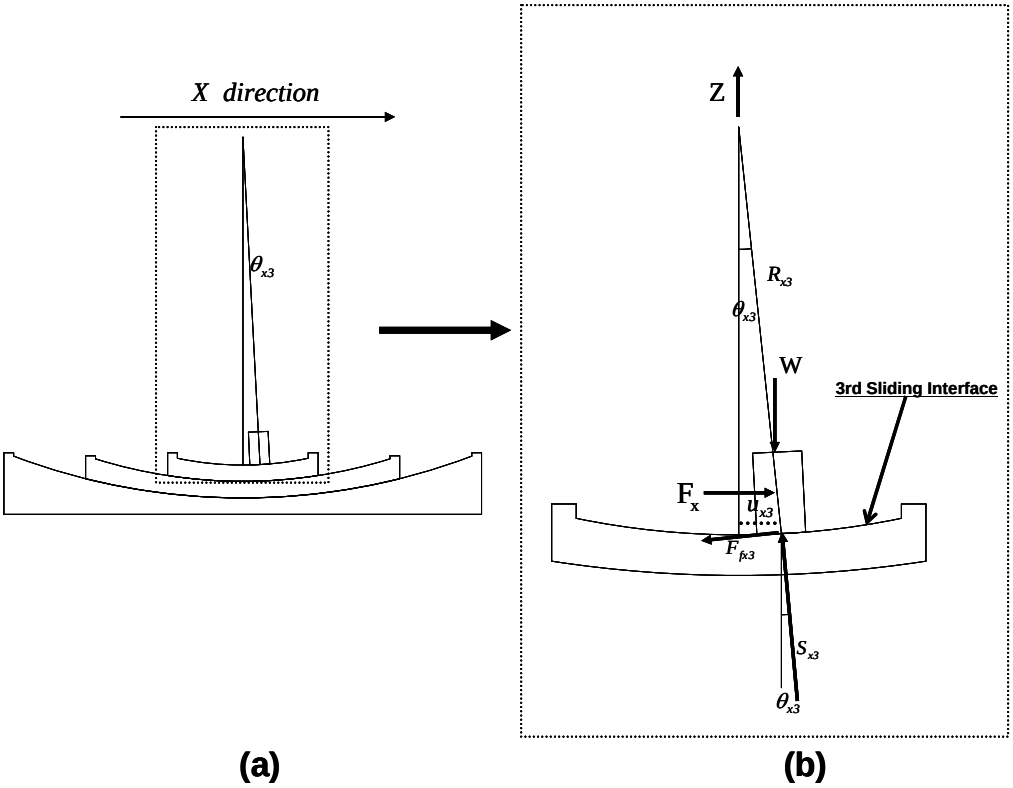

Fig. 7 Displaced positions: (a) free body diagram of MTFPS during sliding Stage I in X-direction, and (b) sliding occurrence on 3rd sliding interface.

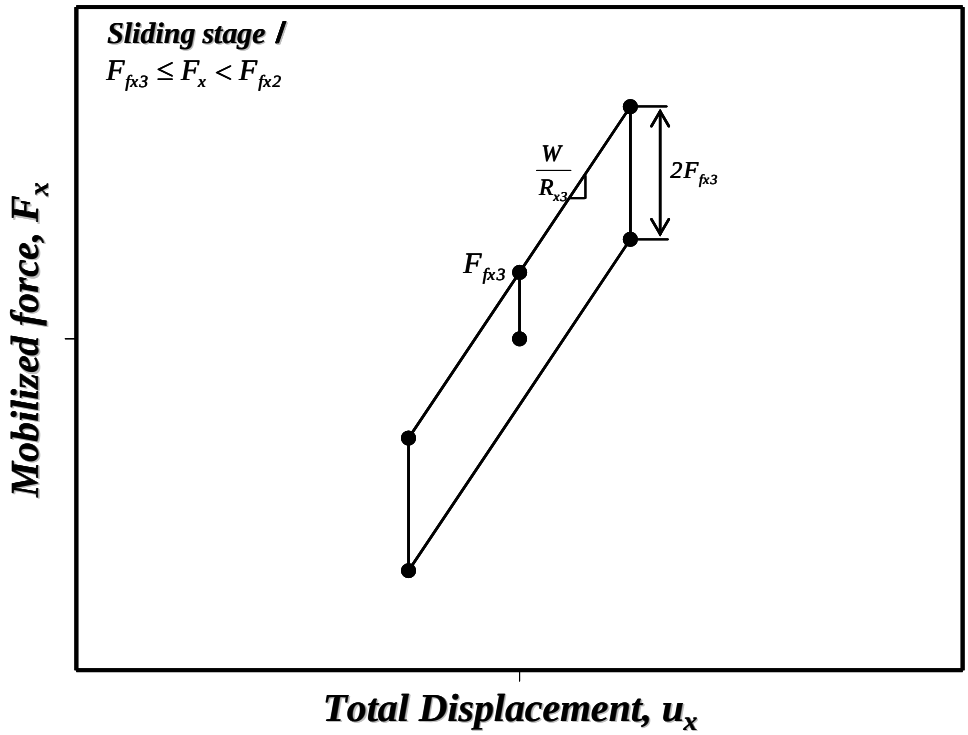

Fig. 8 Force-displacement relationship of the MTFPS isolator during Stage I

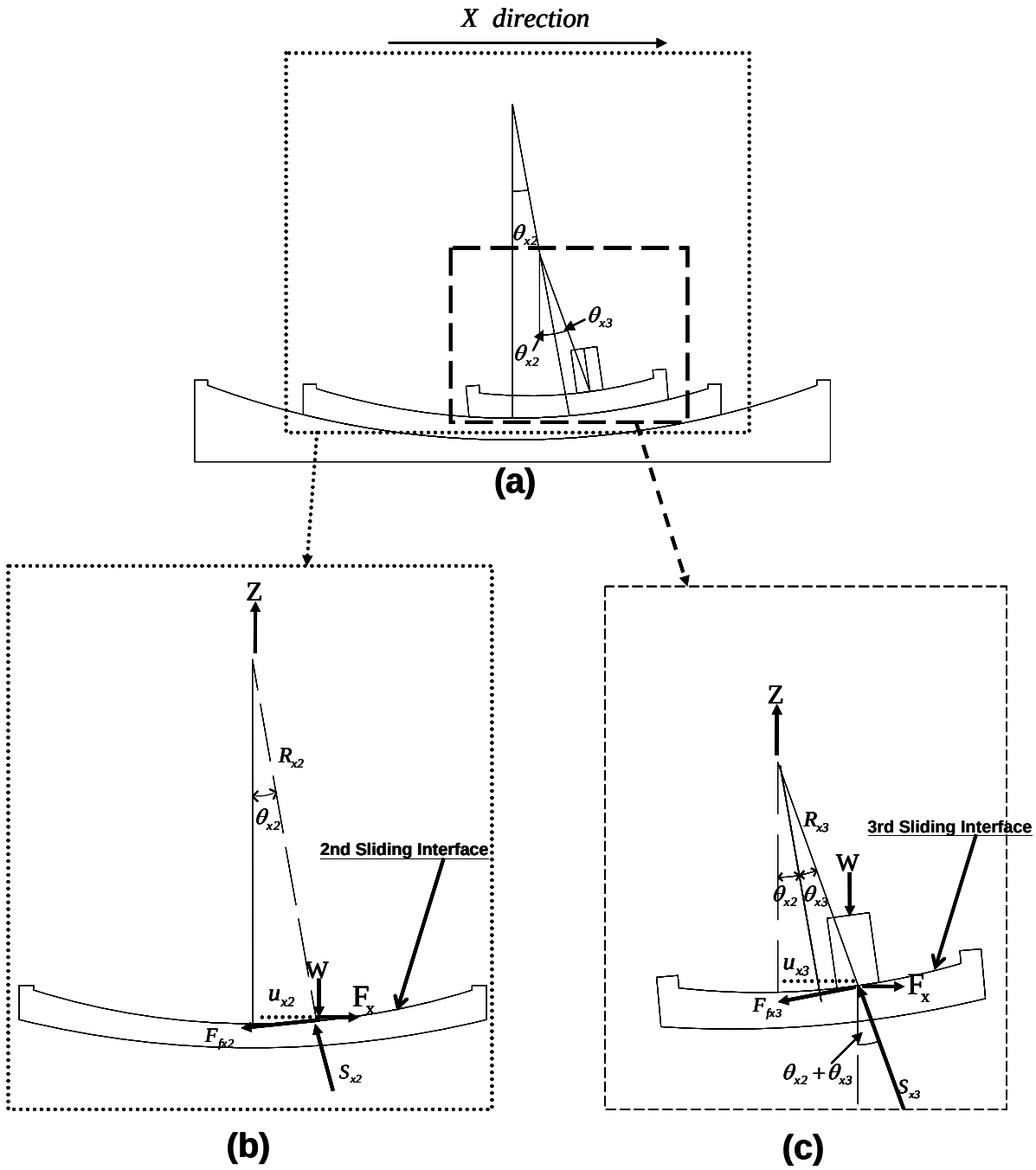

Fig. 9 Displaced positions: (a) free body diagram of the MTFPS during sliding Stage II in X-direction, (b) sliding occurrence on 2nd sliding interface, and (c) a constant displacement on 3rd sliding interface.

.

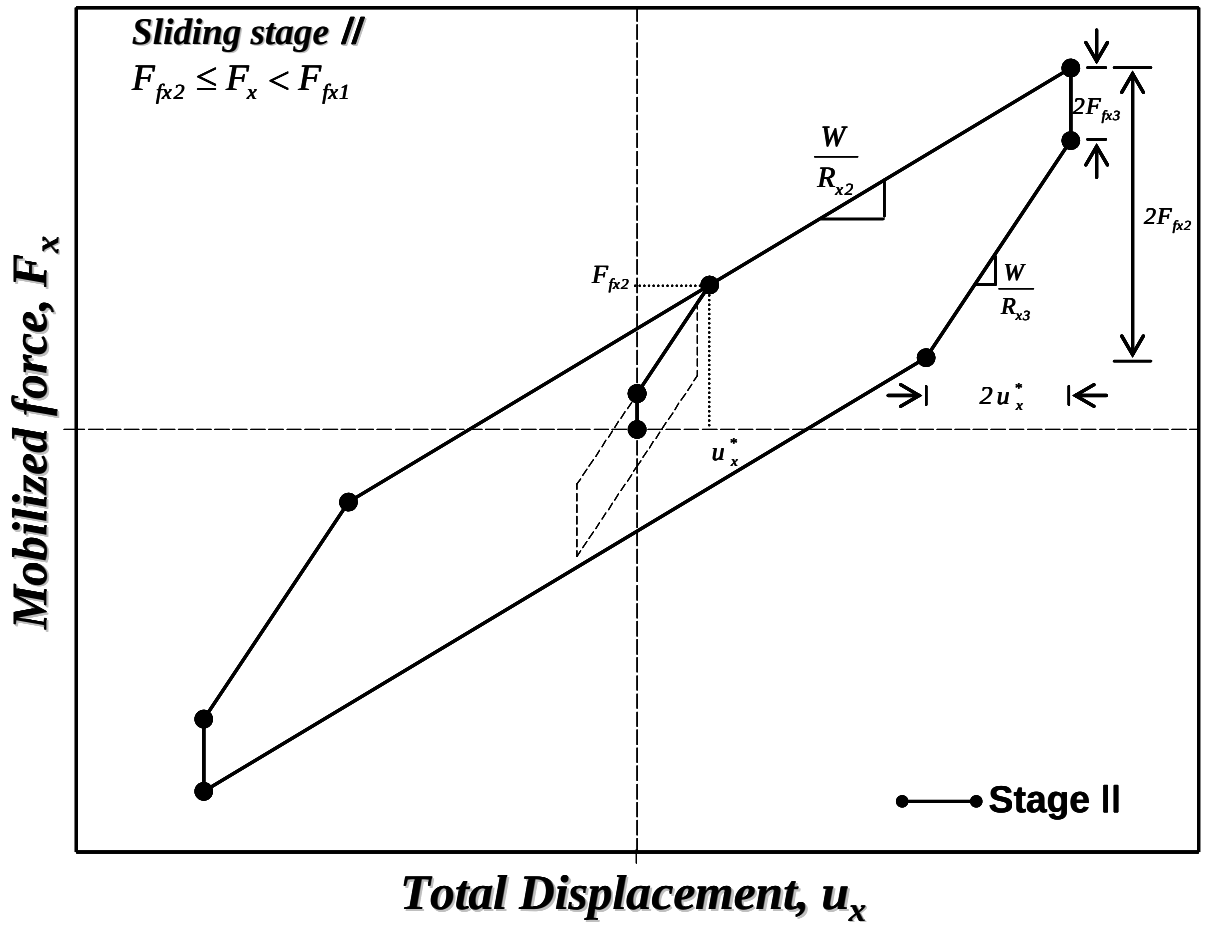

Fig. 10 Force-displacement relationship of the MTFPS isolator during Stage II

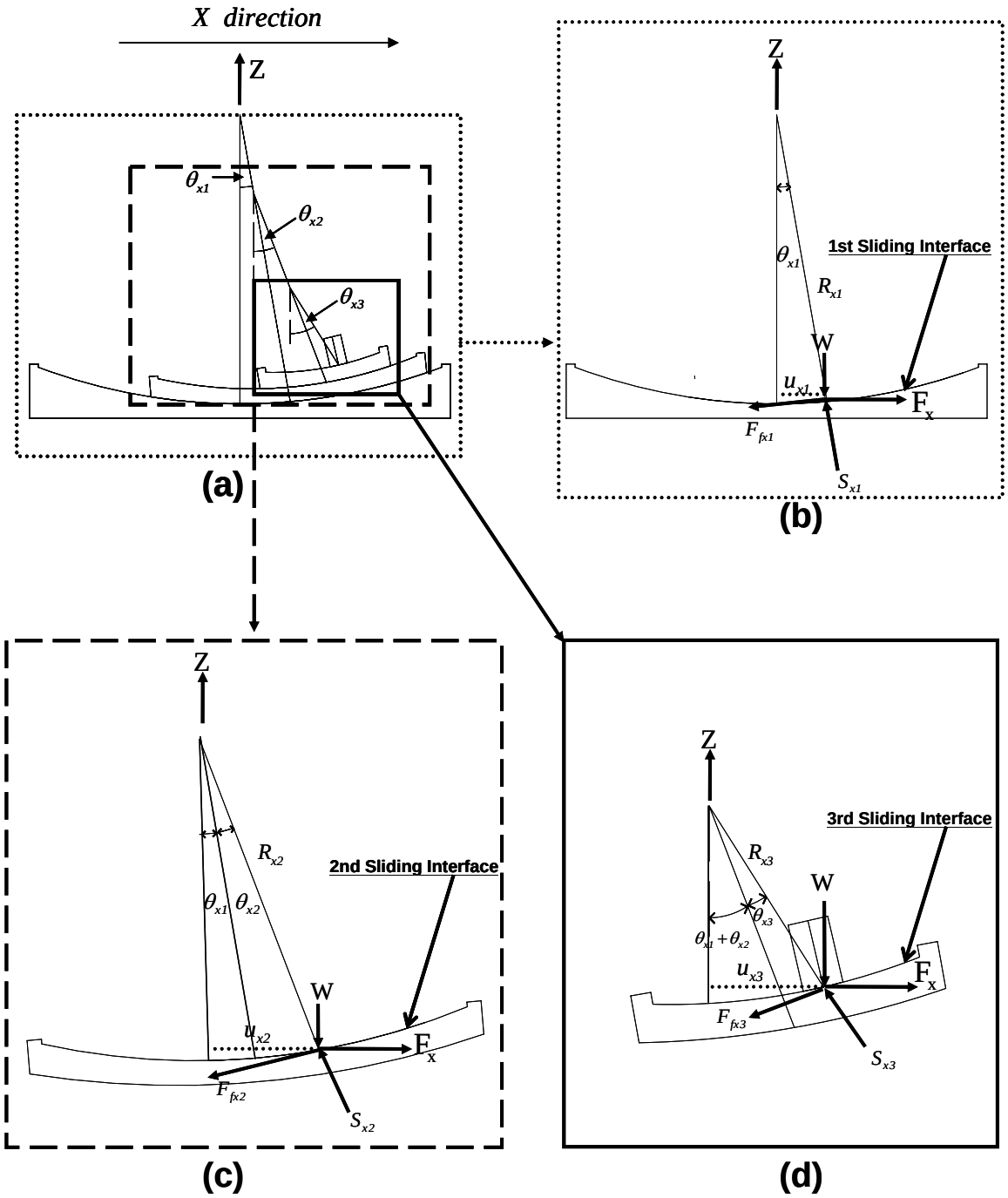

Fig. 11 Displaced positions: (a) free body diagram of the MTFPS during sliding Stage III in X-direction (b) sliding occurrence on 1st sliding interface, (c) a constant displacement on 2nd sliding interface, and (d) a constant displacement on 3rd sliding interface.

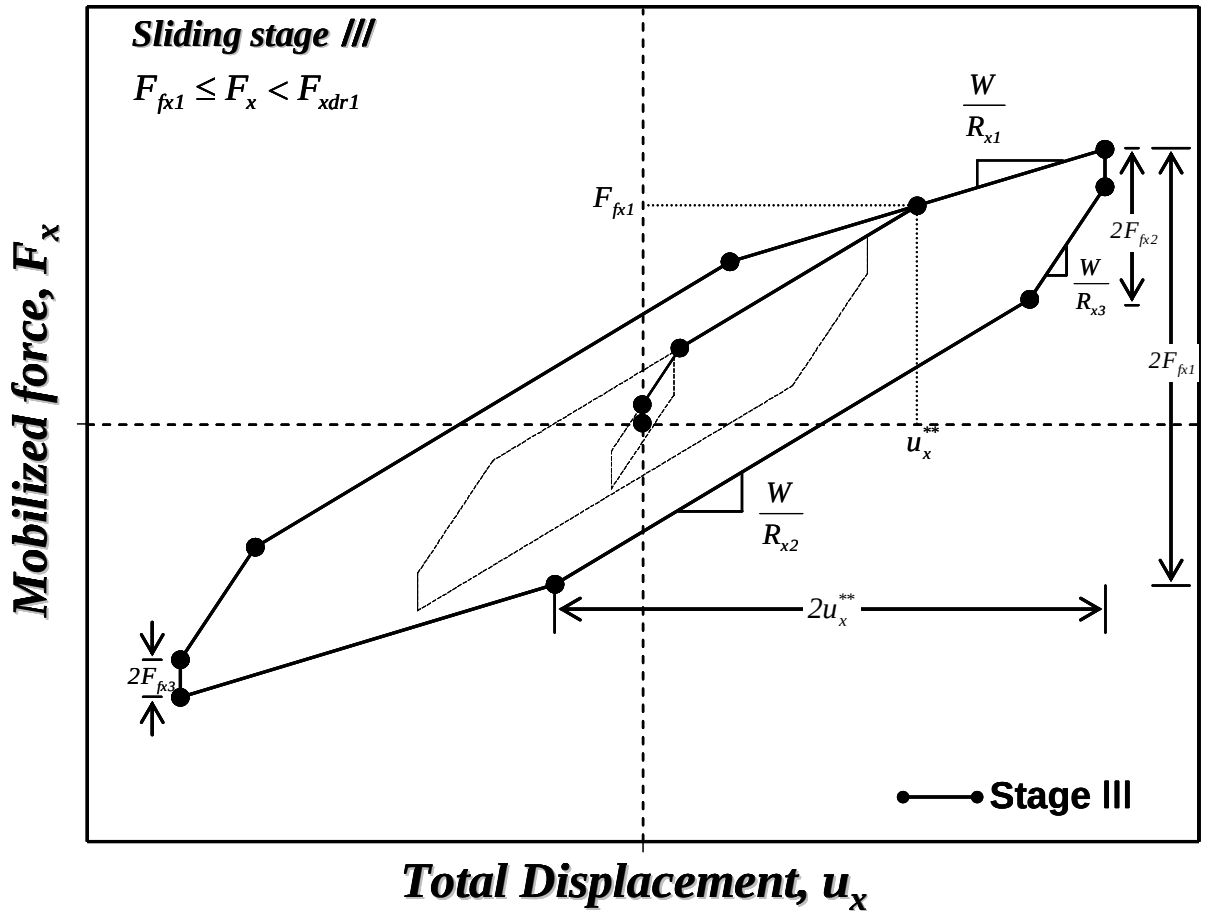

Fig. 12 Force-displacement relationship of the MTFPS isolator during Stage III

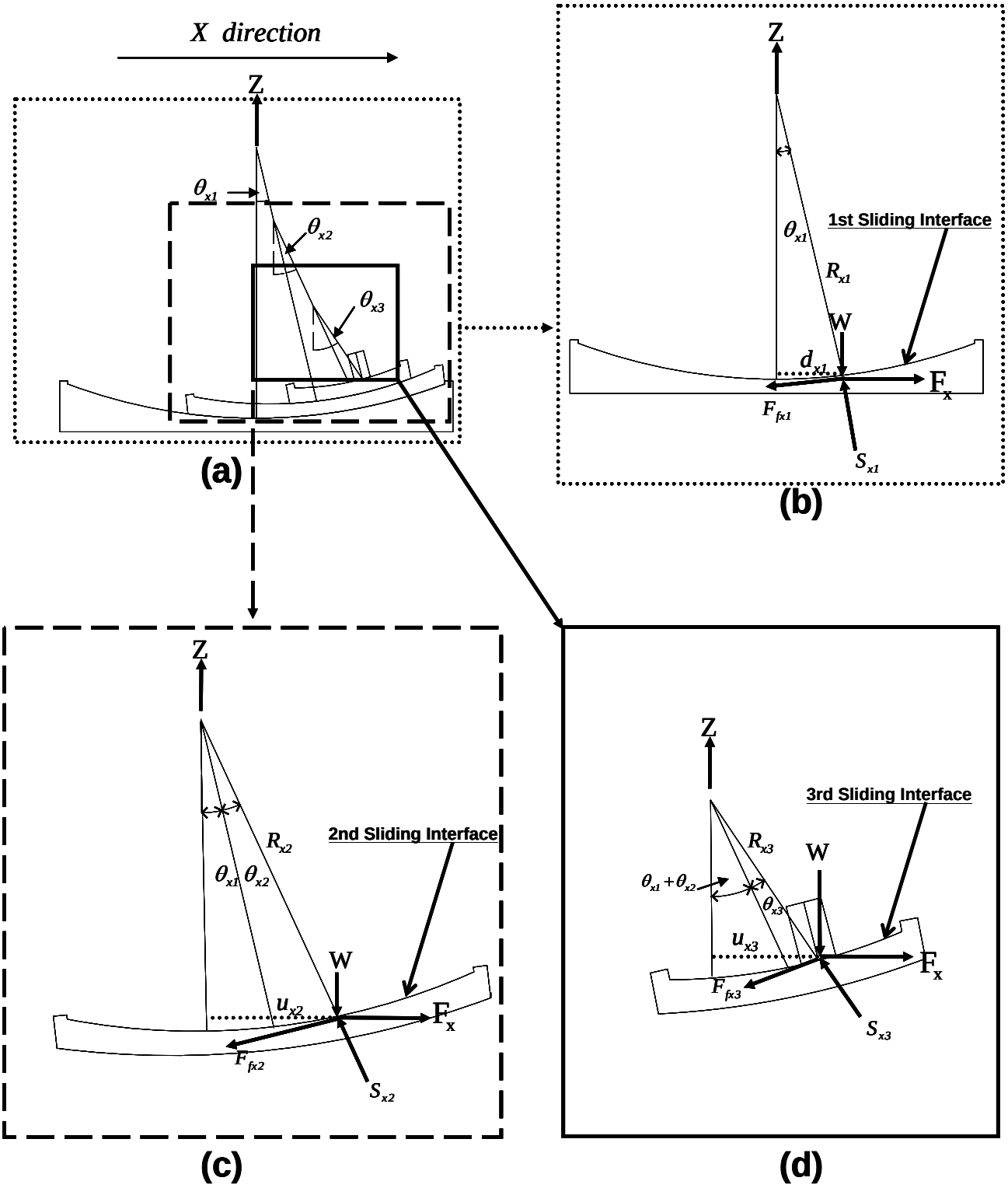

Fig. 13 Displaced positions: (a) free body diagram of the MTFPS during sliding Stage Ⅳ in X-direction, (b) contacting the displacement restrainer on 1st sliding interface, (c) sliding occurrence on 2nd sliding interface, and (d) a constant displacement on 3rd sliding interface.

.

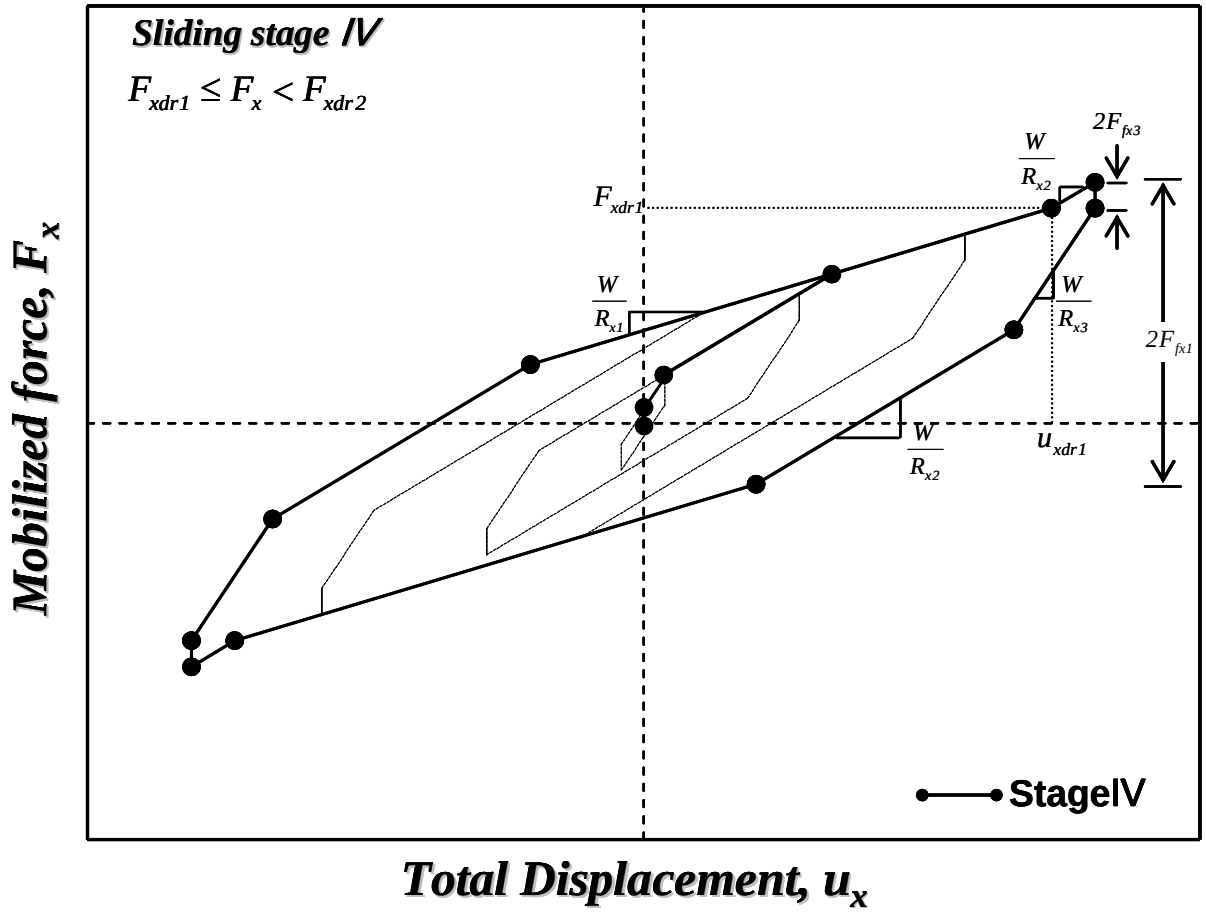

Fig. 14 Force-displacement relationship of the MTFPS isolator during Stage IV

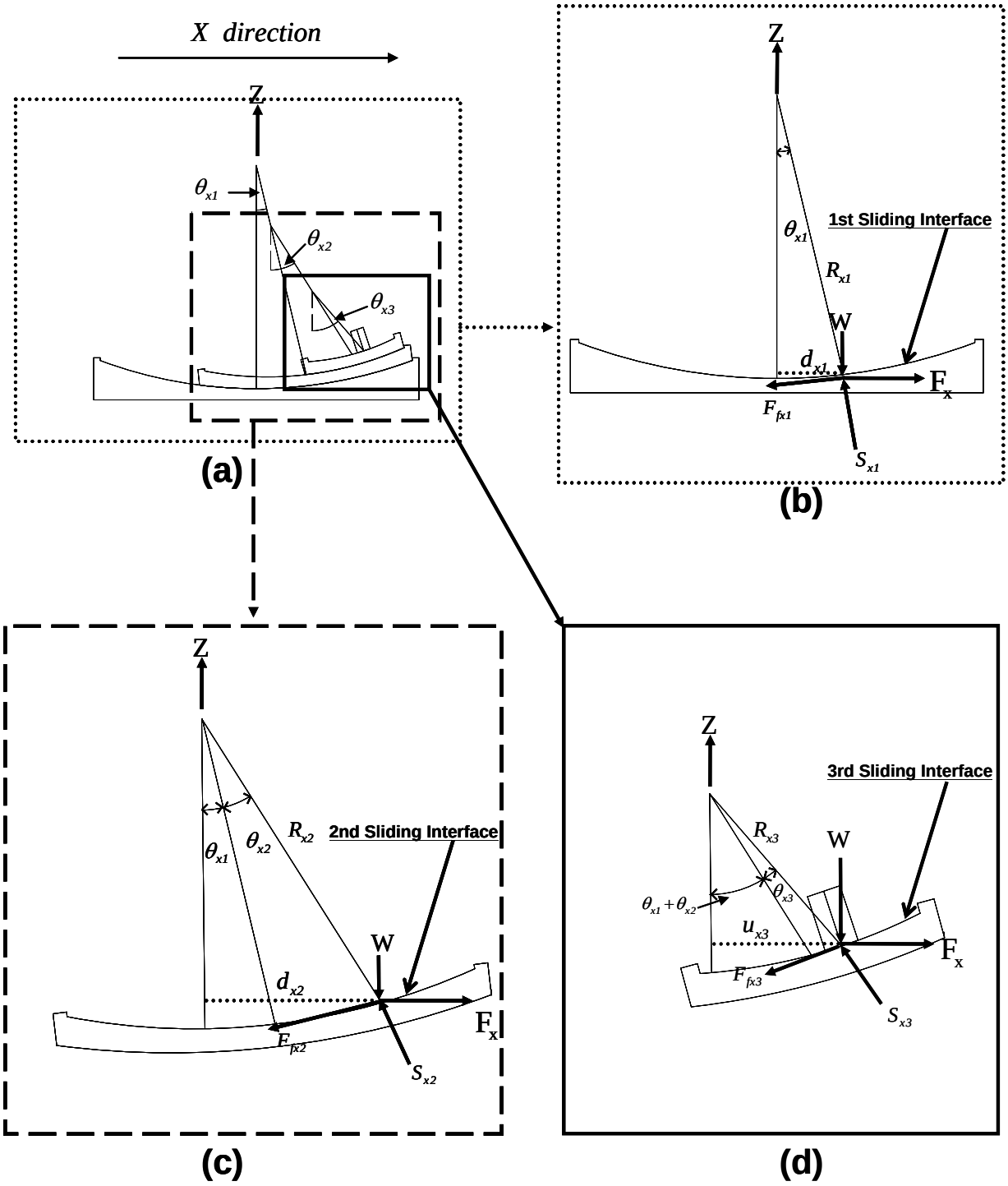

Fig. 15 Displaced positions: (a) free body diagram of the MTFPS during sliding Stage V in X-direction, (b) contacting the displacement restrainer on 1st sliding interface, (c) contacting displacement restrainer on 2nd sliding interface, and (d) sliding occurrence on 3rd sliding interface.

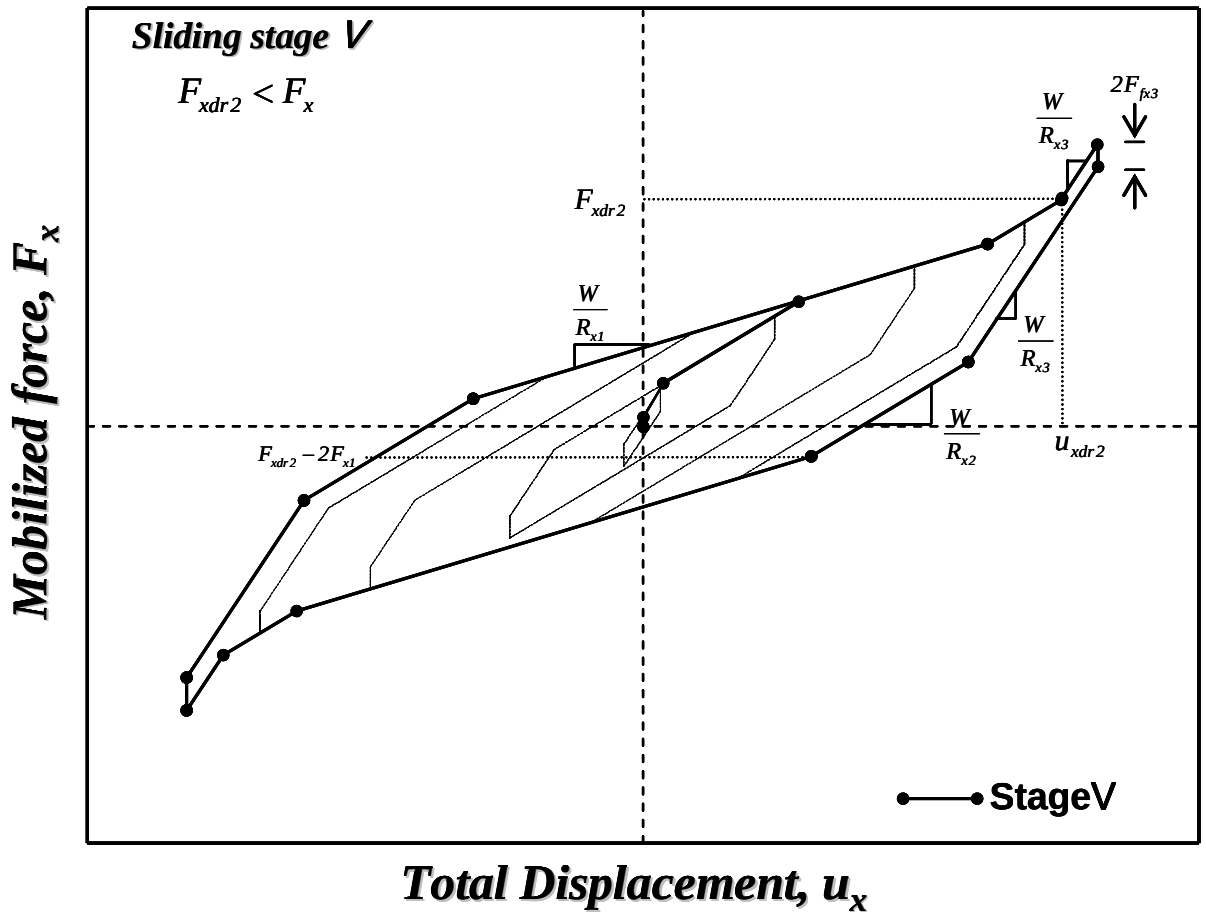

Fig. 16 Force-displacement relationship of the MTFPS isolator during Stage V

Fig. 17 A three story steel structure isolated with four MTFPS isolators

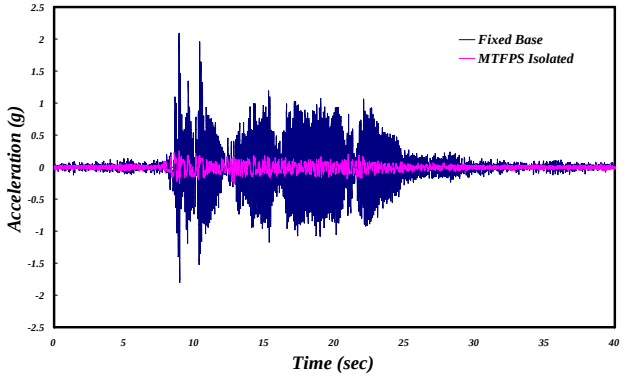

Fig. 18 Comparison of roof acceleration responses of fixed- base and MTFPS-isolated structures under El Centro earthquake with 0.619g in PGA

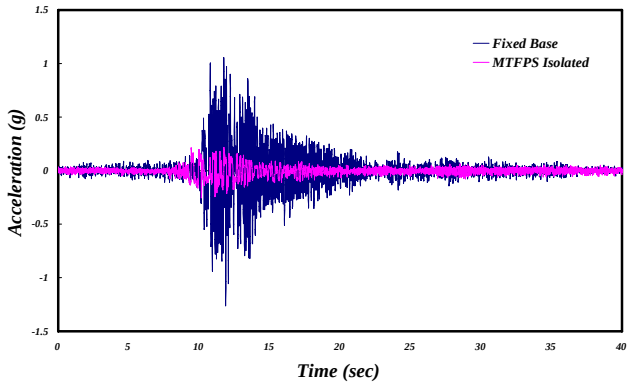

Fig. 19 Comparison of roof acceleration responses of fixed- base and MTFPS-isolated structures under Kobe earthquake with 0.602g in PGA

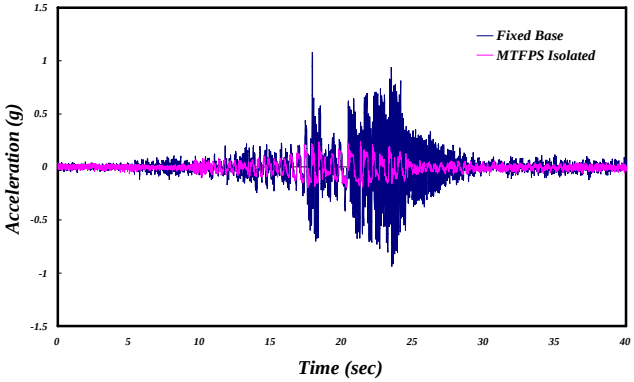

Fig. 20 Comparison of roof acceleration responses of fixed- base and MTFPS-isolated structures under Chi-Chi earthquake with 0.540g in PGA

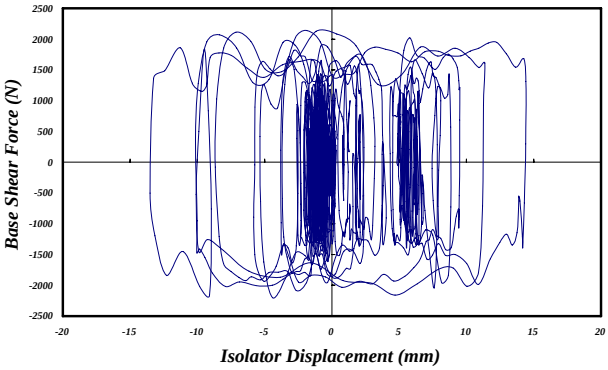

Fig. 21 Hysteresis loops of base isolator under El Centro earthquake with 0.619g in PGA

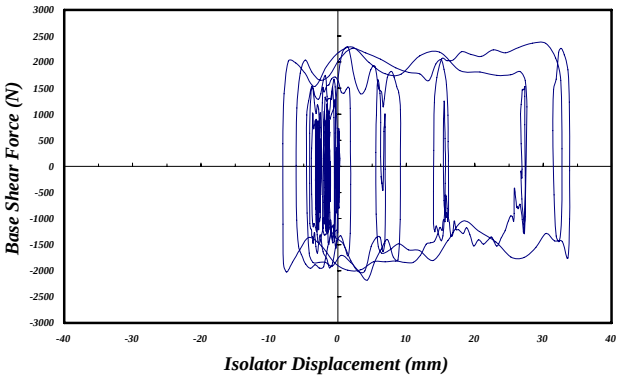

Fig. 22 Hysteresis loops of base isolator under Kobe earthquake with 0.602g in PGA

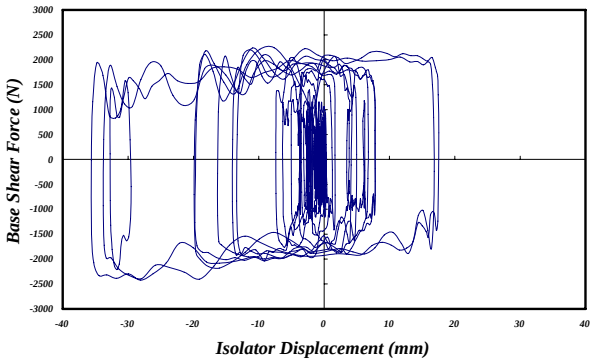

Fig. 23 Hysteresis loops of base isolator under Chi-Chi earthquake with 0.540g in PGA

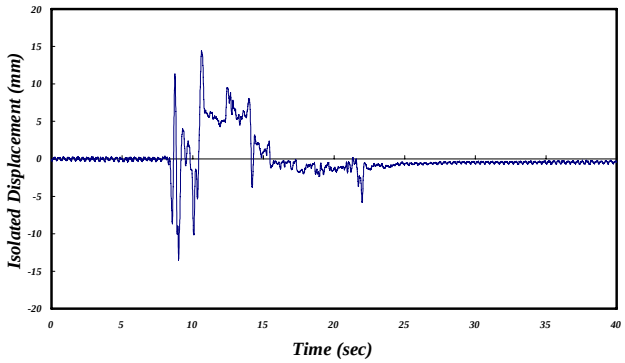

Fig. 24 Time history of isolator displacement under El Centro earthquake with 0.619g in PGA

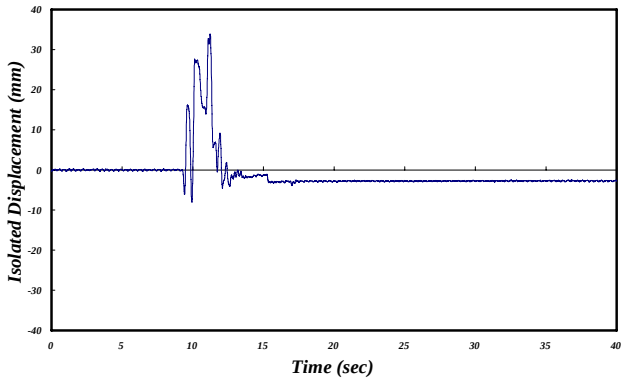

Fig. 25 Time history of isolator displacement under Kobe earthquake with 0.602g in PGA

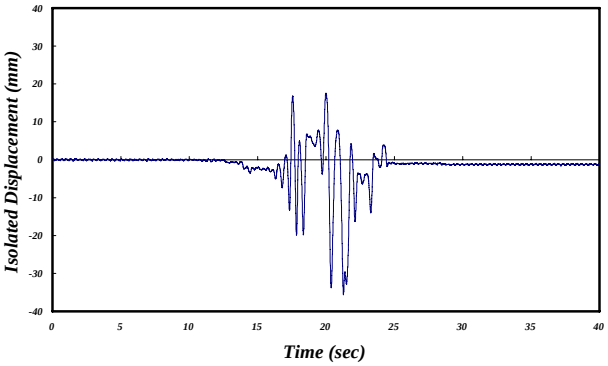

Fig. 26 Time history of isolator displacement under Chi-Chi earthquake with 0.540g in PGA